Localization of Oscillation Source in DC Distribution Network Based on Power Spectral Density

Zida Zhao, Ke Peng, Richang Xian, and Xinhui Zhang

***Abstract*—Direct current (DC) bus voltage stability is essential for the stable and reliable operation of a DC system. If an oscillation source can be quickly and accurately localized, the oscillation can be adequately eliminated. We propose a method based on the power spectral density for identifying the voltage oscillation source. Specifically, a DC distribution network model combined with the component connection method is developed, and the network is separated into multiple power modules. Compared with a conventional method, the proposed method does not require determining the model parameters of the entire power grid, which is typically challenging. Furthermore, combined with a novel judgment index, the oscillation source can be identified more intuitively and clearly to enhance the applicability to real power grids. The performance of the proposed method has been evaluated using the MATLAB/Simulink software and PLECS RT Box experimental platform. The simulation and experimental results verify that the proposed method can accurately identify oscillation sources in a DC distribution network.**

***Index Terms*—Direct current (DC) distribution network, oscillation source, component connection method, power spectral density.**

I. Introduction

In recent years, the access to distributed generation, energy storage, and diversified loads has transformed direct current (DC) distribution networks from static operation structures to flexible and active intelligent structures. In addition, given the absence of fluctuation in reactive power, the DC bus voltage is an essential index to measure secure and stable operation [1].

In a DC distribution network, the lack of rotating equipment (e. g., synchronous generators) and its interconnection with an alternating current (AC) power grid through power electronic devices relatively isolate the inertia, leading to the gradual appearance of voltage oscillation problems [2]. The oscillation mechanism of DC systems has been extensively studied. In [3], the crucial problems of multi-time-scale and random characteristics confronted by a DC system are summarized. In [4] and [5], the influences of loads, converter droop coefficient, and other parameters on high-frequency oscillations are studied. In [6]-[8], based on a reduced-order model, the influences of filter capacitance, controller parameters, and other parameters on bus voltage oscillation are studied. In [9], based on a quasi-linear relationship, a novel extended DC power flow model is proposed. This model is simple, reliable, and precise in standard system operation states. To enhance the stability of a DC distribution network, a multi-time-scale optimal power flow strategy is proposed in [10] for an urban DC distribution network in different operating modes. In [11], a perturb and observe voltage regulator and capacitor compensator circuit are proposed to regulate the voltage while delivering the maximum power at full load. For AC/DC hybrid power grids, a cooperative control method is available to eliminate the DC bus voltage oscillation caused by the access to distributed generation, energy storage, and other components [12], [13].

Continuous and unexpected power system oscillations may restrict the transmission capacity in a power grid, possibly leading to serious accidents and large economic losses. To prevent these consequences, an efficient measure is timely localizing the equipment causing the oscillation to take control countermeasures. Research on localization of oscillation source mainly focuses on AC systems. The related methods include the energy function [14]-[17], modal estimation [18]-[21], frequency-domain relation [22]-[24], and damping torque analysis methods [25], whose advantages and disadvantages are listed in Table I.

In the energy function method, a Lyapunov function is applied to an electric power system [14]. In [15] and [16], the dissipating energy flow (DEF) and its practical calculation are introduced, and a wide-area measurement system is used to calculate the energy flow to localize the oscillation sources. A cutset energy scheme is available to use wide-area measurement system data to localize the oscillation source [17]. Modal estimation allows to localize the oscillation source according to the amplitude and phase of each node mode [18]. This method has been applied to analyze the resonance characteristics of an accident related to the oscillation in an

Manuscript received: July 17, 2022; revised: November 5, 2022; accepted: December 6, 2022. Date of CrossCheck: December 6, 2022. Date of online publication: January 27, 2023.

This work was supported in part by the National Natural Science Foundation of China (No. 51807112).

Z. Zhao, K. Peng, R. Xian (corresponding author), and X. Zhang are with the Shandong University of Technology, Zibo, China (e-mail: zzd17865917686@163.com; pengke@sdut.edu.cn; xianrc@163.com; zhxh@sdut.edu.cn).

DOI: 10.35833/MPCE.2022.000423

American system. To capture nonlinear characteristics, a differential equation is linearized in [19] by using a high-order Taylor series, and the oscillation source is localized using modal series characteristics. However, when applying modal estimation for localizing an oscillation source, the identified modal information may lead to miscalculations [20], [21]. The frequency-domain relation method can localize the oscillation source by analyzing the relationship between the transfer function and response. Each generator is assumed to be a potential oscillation source, and the oscillation sources are identified through the error between the input and actual values [22]. In [23], by studying the transfer function between nodes, a node with a phase angle advance is considered to be closer to the oscillation source. In [24], a transfer function matrix of the oscillation source is considered to be diagonally dominant, and the generator prime mover and governor with the maximum power spectral density (PSD) are the oscillation sources. To apply the damping torque method to localize the oscillation source, the generator torque can be decomposed into damping and synchronous torques, and the localization index of oscillation source is obtained [25]. These methods have a clear and intuitive theoretical basis but rely on the acquisition of detailed models for the entire network. To address this challenge, we propose a method for localizing oscillation source in a DC distribution network based on the PSD.

TABLE I
ADVANTAGES AND DISADVANTAGES OF MAIN LOCALIZATION METHODS

Method	Advantage	Disadvantage
Energy function method	Clear in concept, convenient for practical application	Dissipated energy can be generated through non-oscillatory sources, which may lead to misjudgment
Modal estimation method	Suitable for multi-mode oscillation	Identified modal information may be misjudged
Frequency-domain relation method	Simple and easy to perform	Parameters of the whole network model are required
Damping torque analysis method	Clear and appropriate physical interpretation	Detailed model and accurate parameters need to be obtained

The main contributions of this paper are summarized as follows.

1) Based on the component connection method, the node impedance of the DC distribution network is separated from each power module (PM), and a two-port model is established. This model reduces the calculation burden. Furthermore, as each PM is a potential oscillation source, the oscillation source can be identified simply and intuitively based on the established model.

2) Based on the PSD, we propose a method for localizing the oscillation source. Compared with a conventional method, the proposed method does not require the parameters of the entire power grid model, and the PSD of each PM can be obtained by using its input signal and transfer function. Furthermore, when combined with a proposed judgment index, the oscillation source can be localized more intuitively and clearly.

3) Equivalent models of diverse DC distribution networks are constructed in the MATLAB/Simulink software using hardware-in-the-loop. Then, the performance of multivariate empirical mode decomposition (MEMD) [26] and the proposed method are compared. The results demonstrate that the proposed method can substantially improve the accuracy and efficiency of oscillation source localization.

The remainder of this paper is organized as follows. In Section II, a model of the DC distribution network is presented. In Section III, based on the PSD, the method for oscillation source localization is detailed. In Section IV, the theoretical analysis is validated through case studies including simulation and experimental analyses. Finally, conclusions are drawn in Section V.

II. MODEL OF DC DISTRIBUTION NETWORK

The research object for this paper is a DC distribution network with multiple sources. The system is powered by an AC system through converters and comprises distributed generation, energy storage (ES), AC loads, electric vehicles (EVs), and other components. A schematic of a typical DC distribution network topology with two sources is shown in Fig. 1.

The converters that interact between the AC and DC systems adopt the droop control, which has a simple structure and can realize reasonable power allocation [27]. Because distributed generation adopts the maximum power tracking control, ES and EVs can balance the system power. As the AC load generally adopts constant power control, each unit can be equivalent to a constant power load (CPL). We use a series resistance converter to represent the CPL.

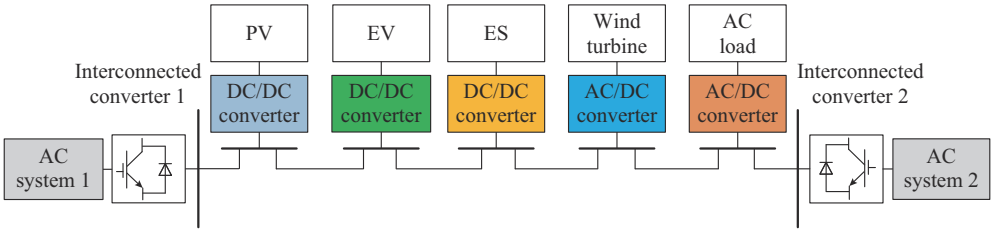

Fig. 1. Schematic of a typical DC distribution network topology with two sources.

The schematic of a simplified model of the DC distribution network with multiple sources is shown in Fig. 2, where u_j $(0<j\le k)$ is the equivalent voltage of the three-phase source; $u_{j,\mathrm{o}}$ is the equivalent voltage on the AC side; R_j and L_j are the equivalent impedances; $I_{j,\mathrm{dc}}$ is the output current of the inverters; $I_{j,\mathrm{L}}$ is the equivalent current of the DC load;

$C_{j,\mathrm{dc}}$ is the filter capacitor on the DC side; $load_j$ ($k<j\le N$) and its converter are the CPLs; N is the number of nodes; and VSC stands for voltage source converter.

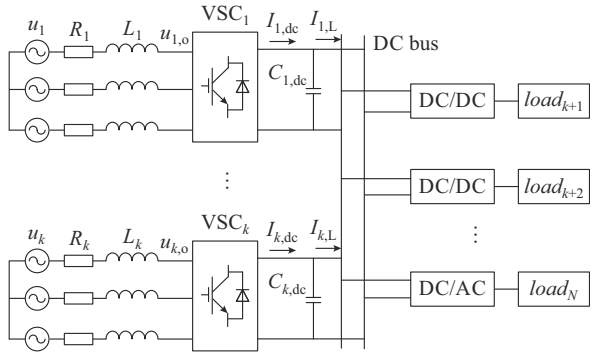

Fig. 2. Schematic of simplified model of DC distribution network with multiple sources.

Because sources and CPLs are connected to a DC distribution network through converters, they can be represented by a PM. Taking the PM as the basic unit, we apply the component connection method to model the DC distribution network [28]-[30]. The schematic of the Norton equivalent model is shown in Fig. 3. When establishing the equivalent model, two-port models are developed for each PM and the system node impedance. The PM can be described by Norton's theorem.

Suppose that AC power sources are connected to nodes numbered from 1 to k, and CPLs are connected to nodes numbered from $k+1$ to N. The connection line between the PMs adopts a π-type centralized equivalent model. Taking the connection line between nodes 1 and 2 as an example, $r_{l,12}$ is the line resistance; $L_{l,12}$ is the line inductance; and $C_{l,12}$ is the line equivalent capacitance. In each PM, $U_{j,\mathrm{dc}}$ is the DC voltage; Z_{u_j} is the output impedance of the source; Y_j is the input admittance of a CPL; $Y_{j,l}$ is the node admittance; $I_{j,\mathrm{ref}}$ and $U_{j,\mathrm{ref}}$ are the reference current and voltage, respectively; and $G_{j,\mathrm{pc}}$ and $G_{j,\mathrm{pd}}$ are the closed-loop transfer functions of source and CPL equivalent models, respectively.

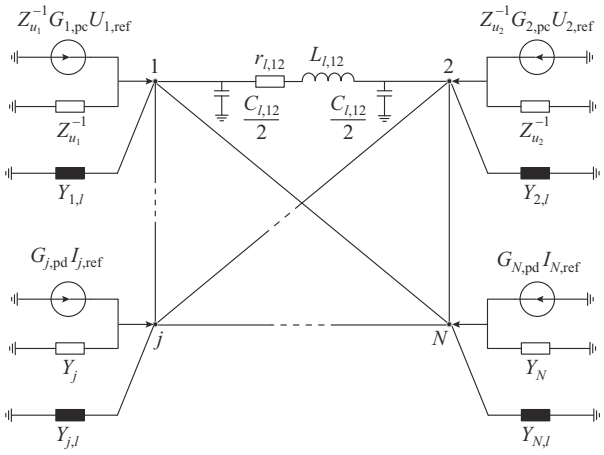

Fig. 3. Schematic of Norton equivalent model.

The droop control structure adopted in this paper for PM$_j$ ($0<j\le k$) is shown in Fig. 4, where $P_{j,\mathrm{ref}}$ and P_j are the reference and measured power values of PM$_j$, respectively; $k_{j,\mathrm{Vp}}$ and $k_{j,\mathrm{Vi}}$ are the proportional and integral coefficients of the outer loop proportional-integral regulator, respectively; $k_{j,\mathrm{Ip}}$ and $k_{j,\mathrm{Ii}}$ are the proportional and integral coefficients of the inner-loop proportional-integral regulator, respectively; k_j and $k_{j,\mathrm{d}}$ are the proportional and droop coefficients, respectively; $u_{j,\mathrm{d}}$ and $i_{j,\mathrm{d}}$ are the d-axis components of the AC-side voltage and current, respectively; $k_{j,\mathrm{ga}}$ is the equivalent gain of the converter; U_j is the DC-side voltage; and s is the Laplace operator.

For the droop control system illustrated in Fig. 4, the closed-loop transfer function of PM$_j$ is given by:

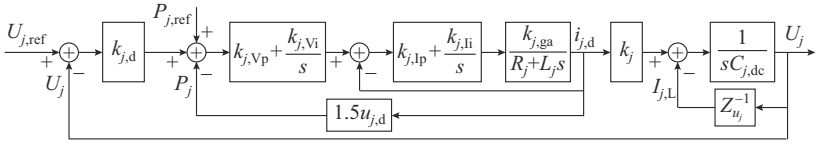

Fig. 4. Droop control structure adopted in this paper.

$$G_{j,\mathrm{pc}}(s)=\frac{G_{j,\mathrm{po}}(s)}{1+1.5u_{j,\mathrm{d}}G_{j,\mathrm{po}}(s)} \tag{1}$$

$$G_{j,\mathrm{I}}(s)=\frac{k_{j,\mathrm{Ip}}k_{j,\mathrm{ga}}s+k_{j,\mathrm{Ii}}k_{j,\mathrm{ga}}}{s^2L+(R+k_{j,\mathrm{Ip}}k_{j,\mathrm{ga}})s+k_{j,\mathrm{Ii}}k_{j,\mathrm{ga}}} \tag{2}$$

$$G_{j,\mathrm{po}}(s)=\frac{(k_{j,\mathrm{Ip}}k_{j,\mathrm{ga}}s+k_{j,\mathrm{Ii}}k_{j,\mathrm{ga}})(sk_{j,\mathrm{Vp}}+k_{j,\mathrm{Vi}})}{s^3L+(R+k_{j,\mathrm{Ip}}k_{j,\mathrm{ga}})s^2+k_{j,\mathrm{Ii}}k_{j,\mathrm{ga}}s} \tag{3}$$

where $G_{j,\mathrm{I}}(s)$ and $G_{j,\mathrm{po}}(s)$ are the current closed-loop and power open-loop transfer functions of the system, respectively.

The output impedance in the equivalent circuit can be expressed as follows:

$$Z_{u_j}^{-1}(s)=\frac{L_jC_js^2+(C_jG_{j,i}(s)k_{j,\mathrm{ga}}U_j+r_jC_j)s}{L_js+r_j+G_{j,i}(s)k_{j,\mathrm{ga}}U_j}+\frac{LG_{j,i}(s)G_{j,u}(s)k_{j,\mathrm{ga}}U_j+1}{L_js+r_j+G_{j,i}(s)k_{j,\mathrm{ga}}U_j} \tag{4}$$

$$G_{j,\mathrm{i}}(s)=k_{j,\mathrm{Ip}}+\frac{k_{j,\mathrm{Ii}}}{s} \tag{5}$$

$$G_{j,\mathrm{u}}(s)=k_{j,\mathrm{Vp}}+\frac{k_{j,\mathrm{Vi}}}{s} \tag{6}$$

where L_j, r_j, and C_j are the inductance, resistance, and capacitance of the filter circuit, respectively; and $G_{j,\mathrm{i}}(s)$ and $G_{j,\mathrm{u}}(s)$ are the current and voltage controllers, respectively.

For the PMs of the CPLs, the closed-loop transfer function and reactance value can be obtained, as detailed in Ap-

pendix A.

The parameters of the equivalent model are obtained using the inverse Laplace transform as follows:

$$G_{j,\mathrm{pc}}(t)=L^{-1}(G_{j,\mathrm{pc}}(s)) \tag{7}$$

$$Z_{u_j}(t)=L^{-1}(Z_{u_j}(s)) \tag{8}$$

$$G_{j,\mathrm{pd}}(t)=L^{-1}(G_{j,\mathrm{pd}}(s)) \tag{9}$$

$$Y_j(t)=L^{-1}(Y_j(s)) \tag{10}$$

III. Oscillation Source Localization

The fundamental reason for DC bus oscillation is the imbalance of energy between the power source and loads [1]. Therefore, for a DC distribution network, when the bus voltage oscillates, each PM is a potential oscillation source. Accordingly, we determine the PSD of each PM output signal, which is regarded as the predicted PSD. Then, a judgment index based on the measured and predicted PSD values is derived to identify the oscillation source.

The equivalent circuits of the power source and CPL are shown in Fig. 5.

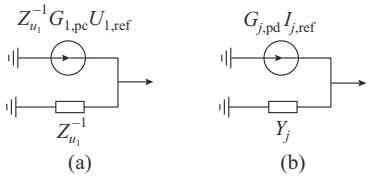

Fig. 5. Equivalent circuits of power source and CPL. (a) Power source. (b) CPL.

According to the equivalent circuit, the input signals of each PM can be expressed as:

$$f_j(t)=\begin{cases}\dfrac{G_{j,\mathrm{pc}}^2(t)U_{j,\mathrm{ref}}^2}{Z_{u_j}(t)} & 0<j\le k\\ \dfrac{G_{j,\mathrm{pd}}^2(t)I_{j,\mathrm{ref}}^2}{Y_j(t)} & k<j\le N\end{cases} \tag{11}$$

where $f_j(t)$ is the input signal of PM$_j$.

In (11), the expressions of $G_{j,\mathrm{pc}}(t)$, $Z_{u_j}(t)$, $G_{j,\mathrm{pd}}(t)$, and $Y_j(t)$ are given during the model setup. Therefore, the input signal of each PM is known. Considering PM$_j$ as an example, the autocorrelation function of the input signal can be expressed as:

$$R_{f_j}(\tau)=\lim_{T\to\infty}\frac{1}{T}\int_{-T/2}^{T/2}f_j(t)f_j(t+\tau)\mathrm{d}t \tag{12}$$

where $R_{f_j}(\tau)$ is the autocorrelation function of the input signal; τ is the independent variable of the autocorrelation function; and T is the period of input signal $f_j(t)$.

During the period of DC system oscillation, the time mean of the input signal autocorrelation function and its PSD are mutual Fourier transforms. Hence, the PSD can be expressed as:

$$s_{f_j}(\omega)=\int_{-\infty}^{\infty}\left(\lim_{T\to\infty}\frac{1}{2T}\int_{-T}^{T}R_{f_j}(t,t+\tau)\mathrm{d}t\right)\mathrm{e}^{-i\omega\tau}\,\mathrm{d}\tau=\int_{-\infty}^{\infty}E(R_{f_j}(t,t+\tau))\,\mathrm{e}^{-i\omega\tau}\mathrm{d}\tau \tag{13}$$

where $E(\cdot)$ is the expectation; $s_{f_j}(\omega)$ is the PSD of input signal $f_j(t)$; and ω is the independent variable of the PSD.

The DC bus voltage oscillation is a generalized stationary random process that satisfies the Wiener-Khinchin theorem. For a stationary (or generalized stationary) random process, the autocorrelation function and PSD of the process are mutual Fourier transforms [31]. Therefore, the PSD of the input signal can be expressed as:

$$s_{f_j}(\omega)=\int_{-\infty}^{\infty}E(R_{f_j}(\tau))\mathrm{e}^{-i\omega\tau}\mathrm{d}\tau=\int_{-\infty}^{+\infty}R_{f_j}(\tau)\mathrm{e}^{-i\omega\tau}\mathrm{d}\tau \tag{14}$$

From the analysis above, the PSD of each PM input signal can be expressed as:

$$\boldsymbol{s}_f=[s_{f_1}(\omega)\quad s_{f_2}(\omega)\quad\cdots\quad s_{f_N}(\omega)]^{\mathrm{T}} \tag{15}$$

For a DC distribution network, the input signal of each PM can be decomposed into a superposition of impulse signals with different time delays. When the input signal is known, the output signal of each PM can be obtained using the continuous-domain convolution. Therefore, the output signal can be expressed as:

$$y_j(t)=f_j(t)*h_j(t)=\int_{-\infty}^{+\infty}f_j(\chi)h_j(t-\chi)\mathrm{d}\chi=\int_{-\infty}^{+\infty}h_j(\chi)f_j(t-\chi)\mathrm{d}\chi \tag{16}$$

where $*$ denotes the convolution operator; $y_j(t)$ is the output signal of PM$_j$; $h_j(t)$ is the impulse response of $y_j(t)$ when $f_j(t)$ is the impulse signal; and χ is an integral variable.

Therefore, the autocorrelation function of the output signal can be expressed as:

$$R_{y_j}(\tau)=\int_{-\infty}^{+\infty}\int_{-\infty}^{+\infty}h_j(\chi_1)h_j(\chi_2)R_{f_j}(\tau-\chi_2+\chi_1)\,\mathrm{d}\chi_1\mathrm{d}\chi_2 \tag{17}$$

where $R_{y_j}(\tau)$ is the autocorrelation function of the output signal of PM$_j$; and χ_1 and χ_2 are integral variables.

According to (14), the PSD of the output signal of PM$_j$ can be expressed as:

$$\begin{aligned}s_{y_j}(\omega)=&\int_{-\infty}^{+\infty}R_{y_j}(\tau)\,\mathrm{e}^{-i\omega\tau}\mathrm{d}\tau\mathrm{d}\chi_1\mathrm{d}\chi_2=\\&\mathrm{e}^{i\omega(\chi_1-\chi_2)}\int_{-\infty}^{+\infty}h_j(\chi_1)\mathrm{d}\chi_1\int_{-\infty}^{+\infty}h_j(\chi_2)\mathrm{d}\chi_2\cdot\\&\int_{-\infty}^{+\infty}\mathrm{e}^{-i\omega(\tau+\chi_1-\chi_2)}R_{f_j}(\tau+\chi_1-\chi_2)\,\mathrm{d}(\tau+\chi_1-\chi_2)=\alpha\eta\end{aligned} \tag{18}$$

$$\alpha=\mathrm{e}^{i\omega(\chi_1-\chi_2)}\int_{-\infty}^{+\infty}h_j(\chi_1)\mathrm{d}\chi_1\int_{-\infty}^{+\infty}h_j(\chi_2)\mathrm{d}\chi_2 \tag{19}$$

$$\eta=\int_{-\infty}^{+\infty}R_{f_j}(\tau+\chi_1-\chi_2)\,\mathrm{e}^{-i\omega(\tau+\chi_1-\chi_2)}\mathrm{d}(\tau+\chi_1-\chi_2) \tag{20}$$

Because the system function can be obtained by Laplace transformation of the impulse response, α can be converted as follows:

$$\begin{cases}\displaystyle\int_{-\infty}^{+\infty}h_j(\chi_1)\mathrm{e}^{i\omega\chi_1}\mathrm{d}\chi_1=G_j^*\\ \displaystyle\int_{-\infty}^{+\infty}h_j(\chi_2)\mathrm{e}^{-i\omega\chi_2}\mathrm{d}\chi_2=G_j\end{cases} \tag{21}$$

where G_j is the transfer function corresponding to the output and input signals of PM$_j$; and G_j^* is the conjugate complex

of G_j.

Through the relationship between the PSD and autocorrelation function in (14), η can be expressed as:

$$\eta = s_{f_j}(\omega) \tag{22}$$

Overall, the PSD of an output signal can be expressed as:

$$s_{y_j}(\omega) = \alpha\eta = s_{f_j}(\omega)\left|G_j\right|^2 \tag{23}$$

where $s_{y_j}(\omega)$ is the PSD of the output signal of PM_j; and $\left|G_j\right|$ is the modulus of transfer function G_j.

Therefore, the output signal PSD of each PM can be expressed as:

$$s_{y_j}(\omega) = \begin{cases} s_{f_j}(\omega)\left|G_{j,\mathrm{pc}}\right|^2 & 0 < j \le k \\ s_{f_j}(\omega)\left|G_{j,\mathrm{pd}}\right|^2 & k < j \le N \end{cases} \tag{24}$$

According to (24), the PSD of each PM can be predicted. Ideally, when the DC bus voltage oscillates, if PM_j is an oscillation source, the measured PSD includes the PSD of the model response and that caused by the disturbance source. Therefore, the predicted PSD differs from the measured one at the oscillation frequency. This condition can be expressed as:

$$s_{y_j}(\omega) \neq s_{y_{j,\mathrm{b}}}(\omega) \tag{25}$$

where $s_{y_{j,\mathrm{b}}}(\omega)$ is the measured PSD of PM_j.

If PM_j is not an oscillation source, the predicted PSD is assumed to be strictly equal to the measured PSD at the oscillation frequency. This condition can be expressed as:

$$s_{y_j}(\omega) = s_{y_{j,\mathrm{b}}}(\omega) \tag{26}$$

However, because several electronic components are connected to the DC distribution network, there are many nonlinear factors, interference noise, and other factors. Therefore, a deviation remains between the predicted and measured PSD values.

Considering the aforementioned factors, we propose the following index θ_j to measure the deviation between the predicted and measured PSD values:

$$\theta_j = \left|1 - \left(\frac{s_{y_j}(\omega)}{s_{y_{j,\mathrm{b}}}(\omega)}\right)^2\right| \tag{27}$$

The judgment index of each PM can be obtained according to (27). If PM_j is an oscillation source, a large deviation between $s_{y_j}(\omega)$ and $s_{y_{j,\mathrm{b}}}(\omega)$ exists, and the proposed index satisfies $\theta_j \gg 0$. Otherwise, the deviation between $s_{y_j}(\omega)$ and $s_{y_{j,\mathrm{b}}}(\omega)$ is small, and the proposed index satisfies $\theta_j \approx 0$.

IV. Case Studies

We report simulation and experimental results that demonstrate the effectiveness of the proposed method for oscillation source localization using the MATLAB/Simulink software and PLECS RT Box experimental platform.

A. Simulation Analysis

To verify the effectiveness of the method to localize an oscillation source, an equivalent model is constructed in MATLAB/Simulink according to the topology of the DC distribution network with two sources, as shown in Fig. 6. The voltage level of the DC bus is 600 V, while G_1 and its converters are PM_1, and G_2 and its converters are PM_2. In addition, variable load $load_3$ and its converters are PM_3, and loads $load_4$-$load_6$ and their converters are PM_4-PM_6. The other parameters are listed in Table II.

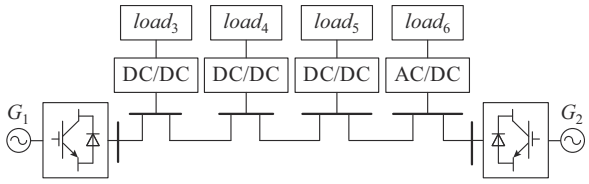

Fig. 6. Topology of DC distribution network for simulation analysis.

TABLE II
Basic Parameters of DC Distribution Network

Parameter	Value	Parameter	Value
$U_{\mathrm{dc,ref}}$	0.6 kV	C_{dc1}, C_{dc2}	4000 μF
u_1, u_2	0.38 kV	$k_{1,\mathrm{Ip}}/k_{1,\mathrm{Ii}}$	1/12
L_1, L_2	2 mH	$k_{2,\mathrm{Ip}}/k_{2,\mathrm{Ii}}$	1/12
R_1, R_2	0.04 Ω	k_1/k_2	4.5
$k_{1,\mathrm{Vp}}/k_{1,\mathrm{Vi}}$	4/50	$k_{1,\mathrm{d}}/k_{2,\mathrm{d}}$	5.5
$k_{2,\mathrm{Vp}}/k_{2,\mathrm{Vi}}$	4/50	$k_{1,\mathrm{ga}}/k_{2,\mathrm{ga}}$	7.3

1) Case 1

Keeping the power consumed by PM_3-PM_6 constant, a disturbance source is connected to PM_1 at 3 s. Because voltage oscillation is induced by the disturbance source connected to PM_1, it is the oscillation source. The voltage oscillation curve of the DC bus for this case is shown in Fig. 7. The oscillation frequency is 8.0 Hz.

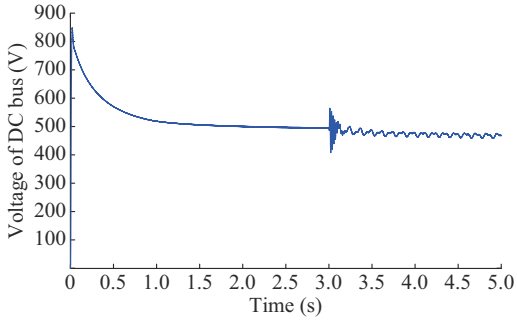

Fig. 7. Voltage oscillation curve of DC bus for simulation case 1.

The measured PSD values of PM_1 and PM_2 are shown in Figs. 8 and 9, respectively. For an oscillation frequency of 8 Hz, the measured PSD values of PM_1 and PM_2 are −16.543 dB/Hz and −15.455 dB/Hz, respectively.

The corresponding judgment indices of PMs are shown in Fig. 10. The judgment index of each PM satisfied $\theta_1 \gg \theta_2 \approx 0$. As PM_2 is not an oscillation source and its measured PSD is approximately equal to the PSD prediction, its judgment index value is approximately equal to zero. On the other hand, PM_1 is the oscillation source, and its measured PSD contains

the predicted PSD that is caused by the disturbance source. Hence, its judgment index is relatively large. Therefore, when the system is connected to an external disturbance source, the results are consistent with theoretical analysis.

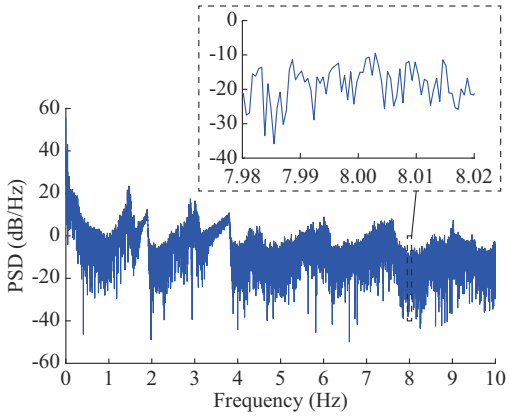

Fig. 8. Measured PSD values of PM_1 for simulation case 1.

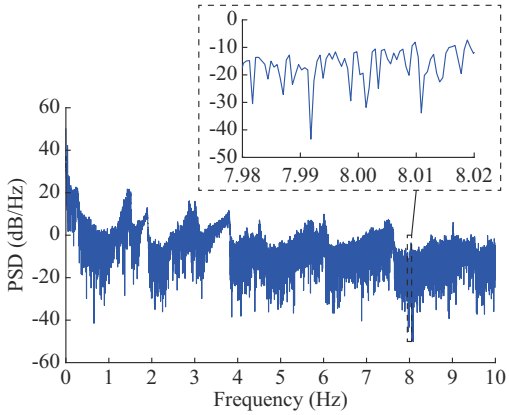

Fig. 9. Measured PSD values of PM_2 for simulation case 1.

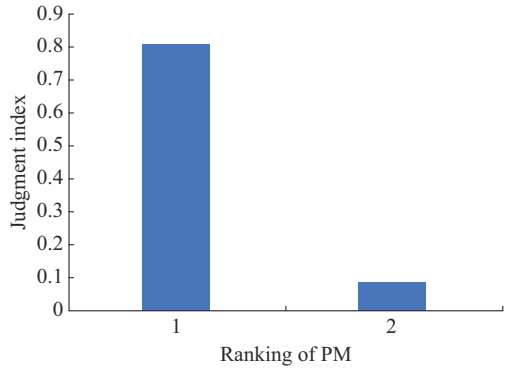

Fig. 10. Judgment indices of PMs for simulation case 1.

MEMD is another method to localize an oscillation source by calculating the variation in DEF, and it combines the energy function method with modal analysis [27]. The DEF curves of each PM are calculated based on the simulation data, obtaining the results shown in Fig. 11. The *y*-axis shows dissipative energy W_{dp}. The DEF curve of PM_1 exhibits an obvious downward trend. Therefore, this method can identify the oscillation source as PM_1, being consistent with the result of the proposed method. However, compared with the proposed method, the conventional MEMD method requires more model parameters, and the model accuracy should be higher, thus being impractical for engineering applications.

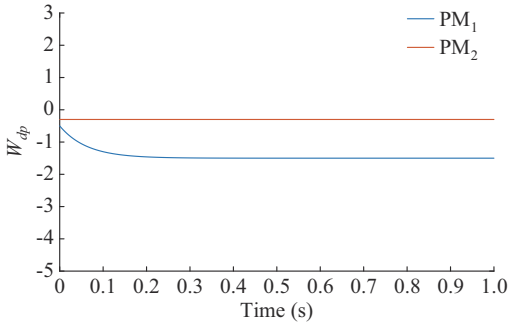

Fig. 11. DEF curves of PMs for simulation case 1.

2) Case 2

Control parameters of PM_3-PM_6 are set to be consistent. The power consumed by PM_4-PM_6 is set to be 30 kW. The initial power consumed by PM_3 is set to be 10 kW, and then the power consumed suddenly changes to 30 kW at 0.6 s, leading to DC bus voltage oscillation.

The voltage oscillation curve of the DC bus is shown in Fig. 12. The oscillation frequency is 43.685 Hz. As the voltage oscillation is induced by a sudden change in the power consumed by PM_3, it is the oscillation source.

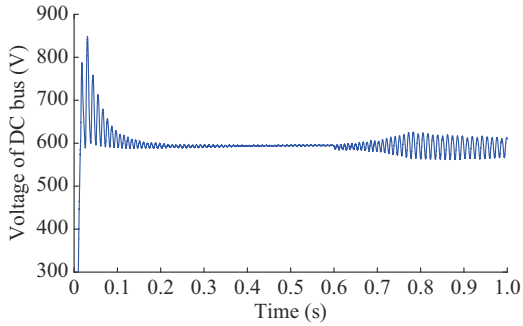

Fig. 12. Voltage oscillation curve of DC bus for simulation case 2.

The measured PSD values of PM_3-PM_6 for simulation case 2 are shown in Figs. 13-16, respectively. When the oscillation frequency is 43.685 Hz, the measured PSD of PM_3 is 5.773 dB/Hz. Because the parameters and states of PM_4-PM_6 are the same, their measured PSD values are all equal to 14.18 dB/Hz.

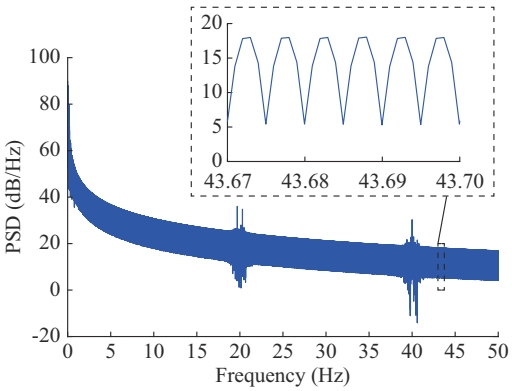

Fig. 13. Measured PSD values of PM_3 for simulation case 2.

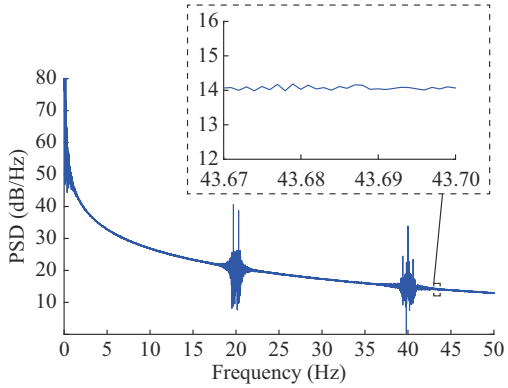

Fig. 14. Measured PSD values of PM_4 for simulation case 2.

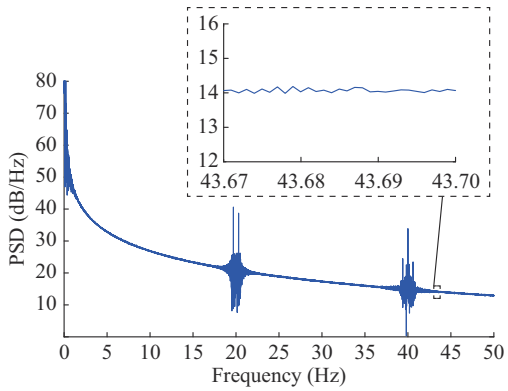

Fig. 15. Measured PSD values of PM_5 for simulation case 2.

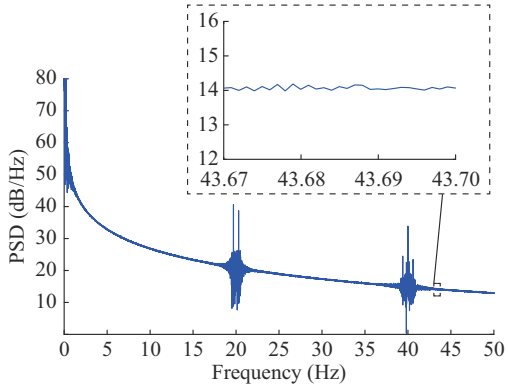

Fig. 16. Measured PSD values of PM_6 for simulation case 2.

The judgment indices and DEF curves of PMs for simulation case 2 are shown in Figs. 17 and 18, respectively. In Fig. 17, the judgment indices of PMs meet $\theta_3 \gg \theta_4 = \theta_5 = \theta_6 \approx 0$. According to theoretical analysis, PM_3 is an oscillation source. However, Fig. 18 shows that the downward trend of DEF curves is very small to identify the oscillation source.

Therefore, when the parameters of each PM are consistent, MEMD could not identify the oscillation source. In contrast, Fig. 17 shows that the proposed method allows to clearly and intuitively identify the oscillation source.

3) Case 3

The power consumed by PM_4-PM_6 is set to be 30 kW, 40 kW, and 50 kW, respectively. The initial power consumed by PM_3 is set to be 10 kW and suddenly changed to 60 kW at 0.6 s, leading to voltage oscillation.

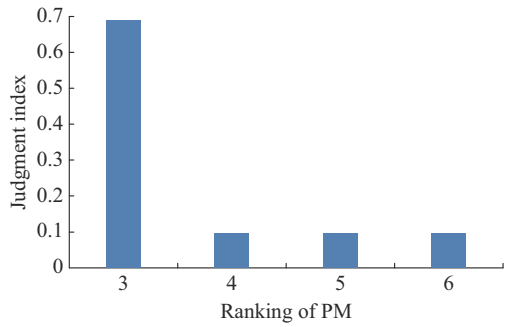

Fig. 17. Judgment indices of PMs for simulation case 2.

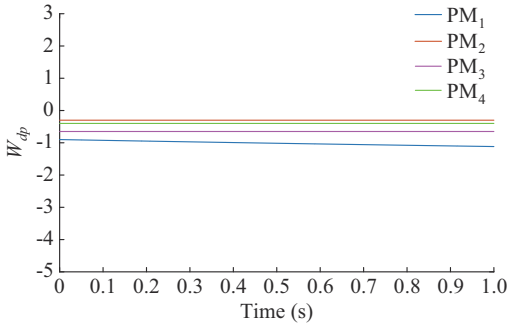

Fig. 18. DEF curves of PMs for simulation case 2.

The voltage oscillation curve of the DC bus is shown in Fig. 19. The oscillation frequency is 40.264 Hz. As the DC voltage oscillation is induced by the sudden change in the power consumed by PM_3, it is the oscillation source.

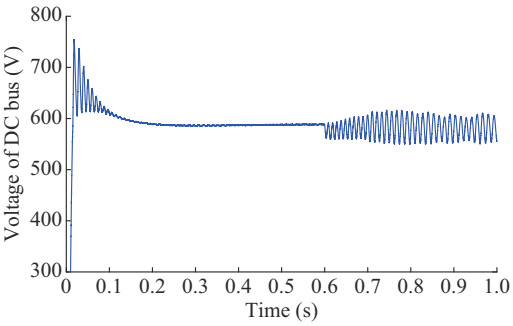

Fig. 19. Voltage oscillation curve of DC bus for simulation case 3.

The measured PSD values of PM_3-PM_6 for simulation case 3 are shown in Figs. 20-23, respectively. When the DC bus voltage oscillation frequency is 40.264 Hz, the measured PSD values of PM_3-PM_6 are 19.857 dB/Hz, 13.446 dB/Hz, 15.945 dB/Hz, and 17.881 dB/Hz, respectively.

The judgment indices and DEF curves of PMs for simulation case 3 are shown in Figs. 24 and 25, respectively. The judgment indices of the PMs meet $\theta_3 \gg \theta_4 \approx \theta_5 \approx \theta_6 \approx 0$. Thus, PM_3 is the oscillation source because its measured PSD has a large deviation from the predicted PSD, and its judgment index is large. Similarly, Fig. 25 shows that the DEF curves exhibit a slight downward trend, hindering the identification of the oscillation source using the conventional method. Compared with Fig. 24, it is difficult or even impossible to identify the oscillation source using MEMD, whereas the

proposed localization method accurately and clearly identifies the oscillation source.

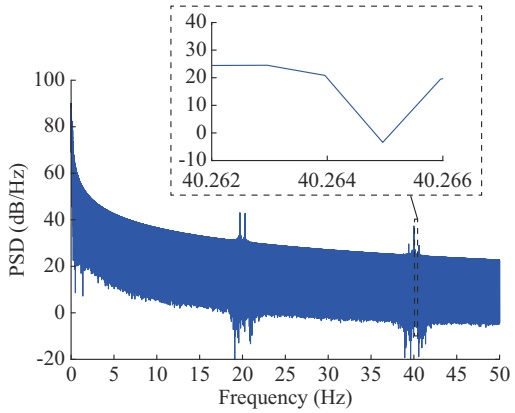

Fig. 20. Measured PSD values of PM_3 for simulation case 3.

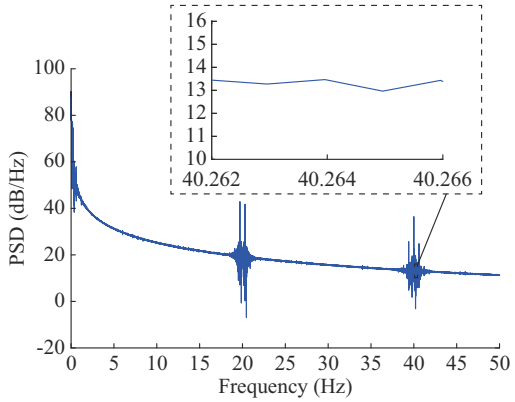

Fig. 21. Measured PSD values of PM_4 for simulation case 3.

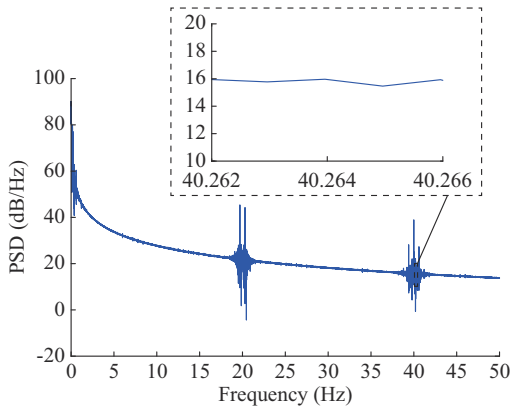

Fig. 22. Measured PSD values of PM_5 for simulation case 3.

By comparing the performances of MEMD and the proposed method, the following results are obtained.

1) For the DC bus voltage oscillation induced by the connected disturbance source, both MEMD and the proposed method can identify the oscillation source. However, MEMD requires relevant parameters of the oscillation dissipation capacity, transient energy variation, and modal decomposition. The proposed method can calculate the PSD for each PM solely by its input signal and transfer function, being more practical for engineering applications.

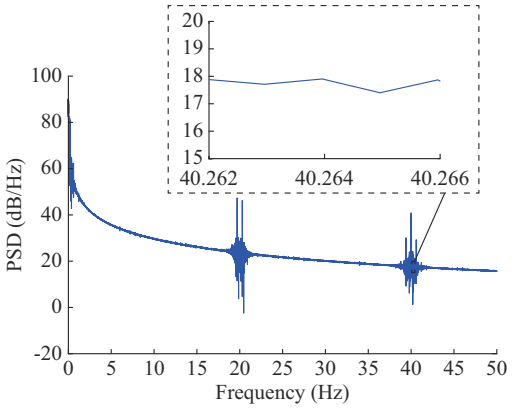

Fig. 23. Measured PSD values of PM_6 for simulation case 3.

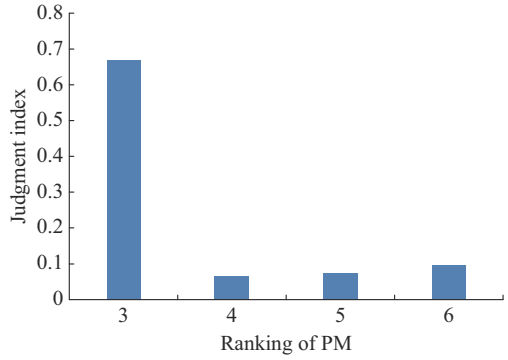

Fig. 24. Judgment indices of PMs for simulation case 3.

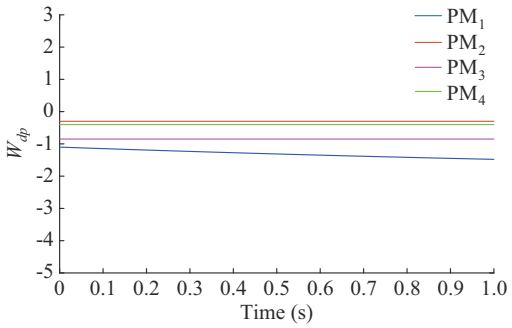

Fig. 25. DEF curves of PMs for simulation case 3.

2) For the DC bus voltage oscillation induced by a sudden change in the load consumption power, cases 1 and 2 show that it is difficult or even impossible to identify the oscillation source using MEMD. In contrast, the proposed method can accurately, clearly, and intuitively identify the oscillation source.

B. Experimental Analysis

The PLECS RT Box experimental platform is equipped with rich digital and analog interfaces, and field-programmable gate array (FPGA) integrated operation modules. It can quickly process real-time models with a hardware-in-the-loop architecture and perform rapid control prototyping. Its results are close to those obtained from an actual power grid. The implementation of RT Box experimental platform used in this paper is shown in Appendix A Fig. A1.

The topology of the DC distribution network for experiment is shown in Fig. 26. The voltage level is set to be 600 V. In addition, G_1-G_3 with their converters are denoted as PM_1-PM_3, respectively, while variable $load_4$ and its converters is denoted as PM_4, and $load_5$-$load_7$ with their converters are denoted as PM_5-PM_7, respectively.

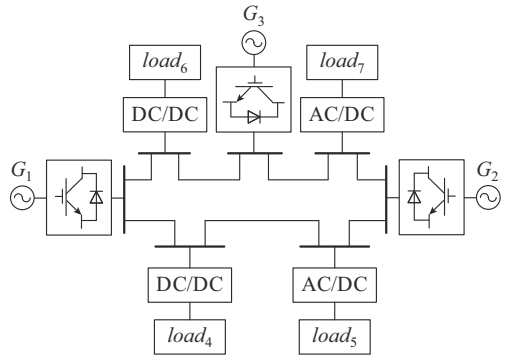

Fig. 26. Topology of DC distribution network for experiment.

1) Case 1

The power consumed by PM_4-PM_7 is constant, and the disturbance source is connected to PM_1 at 1 s. Because voltage oscillation is induced by the disturbance source connected to PM_1, it is the oscillation source. The voltage oscillation curve of the DC bus in this case is shown in Fig. 27 with a frequency of 7.62 Hz.

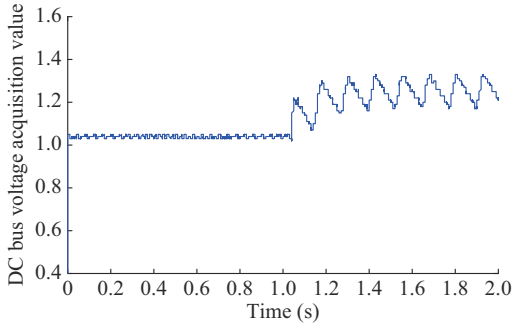

Fig. 27. Voltage oscillation curve of DC bus for experimental case 1.

The measured PSD values of PM_1-PM_3 are shown in Figs. 28-30. When the oscillation frequency is 40.264 Hz, the measured PSD values of PM_1-PM_3 are −39.867 dB/Hz, −43.426 dB/Hz, and −48.952 dB/Hz, respectively.

The judgment indices are shown in Fig. 31. The indices for the PMs meet $\theta_1 \gg \theta_2 \approx \theta_3 \approx 0$. For PM_2 and PM_3, because they are not oscillation sources according to the theoretical analysis, their judgment indices are approximately zero. For the oscillation source in PM_1, its judgment index value is relatively large. Therefore, when the system is connected to an external disturbance source, the results are consistent with the theoretical analysis.

2) Case 2

The power consumed by PM_5-PM_7 is set to be 24 kW, 18 kW, and 24 kW, respectively. The initial power consumed by PM_4 is set to be 18 kW and suddenly changed to 36 kW at 5 s, leading to voltage oscillation.

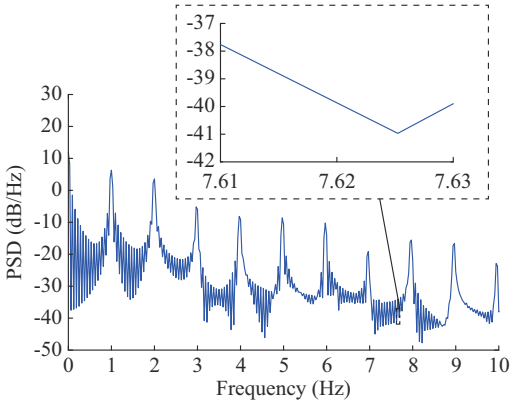

Fig. 28. Measured PSD values of PM_1 for experimental case 1.

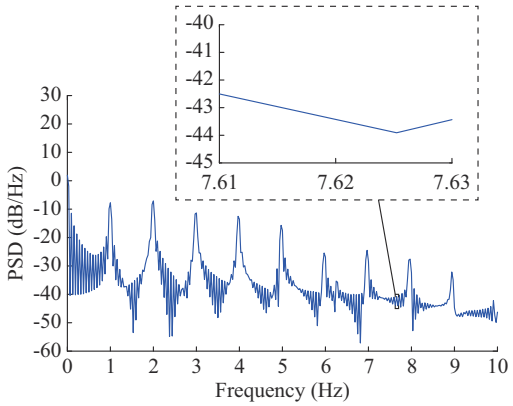

Fig. 29. Measured PSD values of PM_2 for experimental case 1.

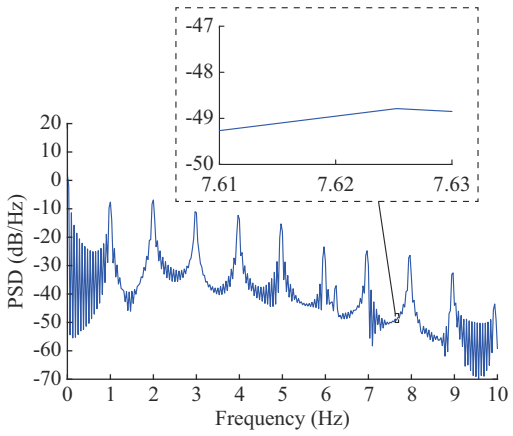

Fig. 30. Measured PSD values of PM_3 for experimental case 1.

The voltage oscillation of the DC bus is shown in Fig. 32. The oscillation frequency is 50.394 Hz. Because the DC voltage oscillation is induced by the sudden change in the power consumed by PM_4, it is the oscillation source.

The measured PSD values of the PMs are shown in Fig. 33-36. When the oscillation frequency is 50.394 Hz, the measured PSD values of PM_4-PM_7 are −55.79 dB/Hz, −68.798 dB/Hz, −57.803 dB/Hz, and −68.794 dB/Hz, respectively.

The judgment indices of PMs are shown in Fig. 37. The judgment indices meet $\theta_4 \gg \theta_5 \approx \theta_6 \approx \theta_7 \approx 0$. Because PM_4 is the oscillation source, its judgment index is relatively large,

while PM_5-PM_7 are not oscillation sources, and their judgment indices are approximately zero. These results are consistent with the theoretical analysis that is presented in Section III.

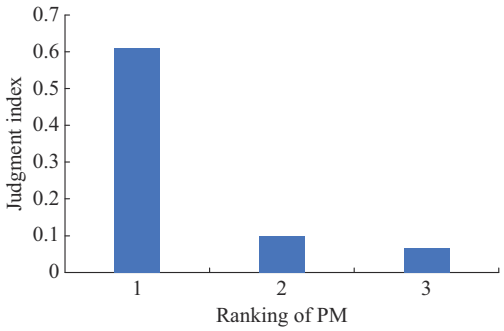

Fig. 31. Judgment indices of PMs for experimental case 1.

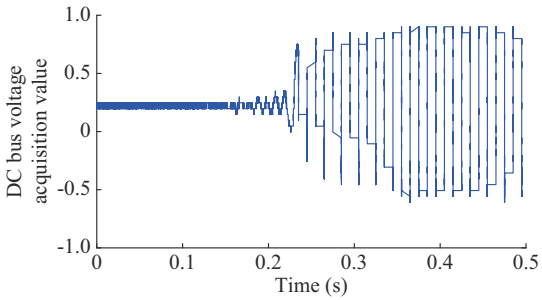

Fig. 32. Voltage oscillation of DC bus for experimental case 2.

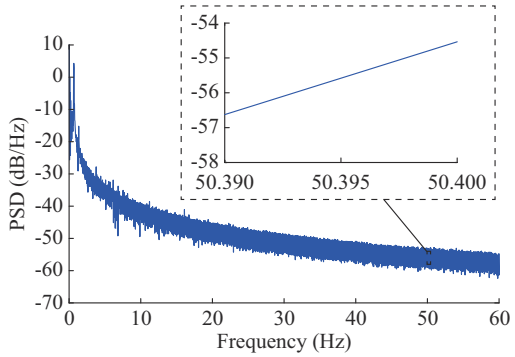

Fig. 33. Measured PSD values of PM_4 for experimental case 2.

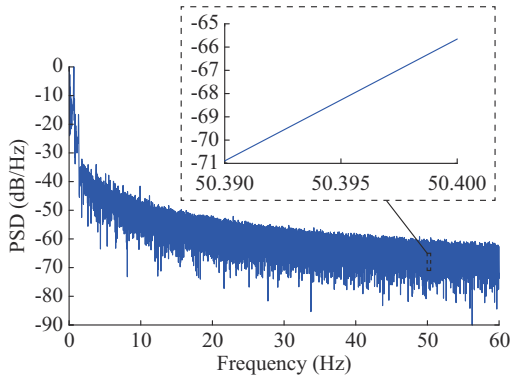

Fig. 34. Measured PSD values of PM_5 for experimental case 2.

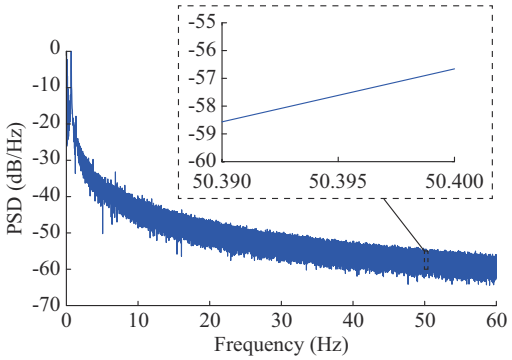

Fig. 35. Measured PSD values of PM_6 for experimental case 2.

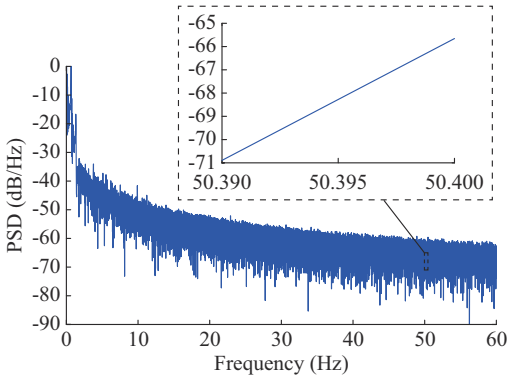

Fig. 36. Measured PSD values of PM_7 for experimental case 2.

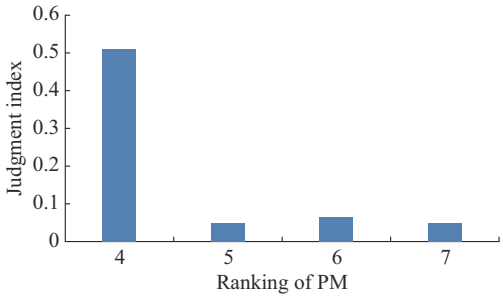

Fig. 37. Judgment indices of PMs for experimental case 2.

V. Conclusion

To address voltage oscillation in a DC distribution network, an immediate and efficient method is localizing the component causing the oscillation timely and accurately to take control countermeasures. Accordingly, we propose an oscillation source localization method for a DC distribution network with multiple sources. The following conclusions can be drawn from the simulation and experimental results.

1) The proposed method does not require a detailed model of the system and can estimate the PSD solely using the input signal of each PM to accurately localize the oscillation source.

2) Compared with a conventional method, the proposed method is suitable for generic DC distribution networks and can accurately identify different types of oscillation sources. Furthermore, when combined with the proposed judgment index, the oscillation source can be identified intuitively and clearly.

3) The proposed method considerably improves the accuracy and efficiency of oscillation source localization, likely providing a reference for power grid operators to formulate relevant control strategies with practical engineering applicability.

APPENDIX A

The Norton equivalent admittance of a CPL is given by:

$$Y_j(s)=\frac{a_{j,4}s^4+a_{j,3}s^3+a_{j,2}s^2+a_{j,1}s^1+a_{j,0}}{b_{j,5}s^5+b_{j,4}s^4+b_{j,3}s^3+b_{j,2}s^2+b_{j,1}s^1+b_{j,0}} \tag{A1}$$

$$G_{j,\mathrm{d}}(s)=k_{j,\mathrm{dp}}+\frac{k_{j,\mathrm{di}}}{s} \tag{A2}$$

$$a_{j,0}=d^2-G_{j,\mathrm{d}}(s)I_j k_{j,\mathrm{da}}R_j d \tag{A3}$$

$$a_{j,1}=G_{j,\mathrm{d}}(s)k_{j,\mathrm{da}}R_j+R_jC_jd^2+R_j+r_j-R_jG_{j,\mathrm{d}}(s)I_j k_{j,\mathrm{da}}d \tag{A4}$$

$$a_{j,2}=R_j(G_{j,\mathrm{d}}(s)k_{j,\mathrm{da}}+C_jd^2)+R_j+r_j+L_j+C_jR_jr_j \tag{A5}$$

$$a_{j,3}=L_j+C_jR_jr_j+C_jL_jr_j \tag{A6}$$

$$a_{j,4}=L_jC_jR_j \tag{A7}$$

$$b_{j,0}=R_j(1+G_{j,\mathrm{d}}(s)k_{j,\mathrm{da}})+r_j \tag{A8}$$

$$b_{j,1}=R_j(1-dI_{j,\mathrm{c}})G_{j,\mathrm{d}}(s)k_{j,\mathrm{da}}+d^2+R_jC_jr_j+R_j+r_j \tag{A9}$$

$$b_{j,3}=R_jG_{j,\mathrm{d}}(s)k_{j,\mathrm{da}}+R_j+r_j+R_jC_j(r_j+L_j+d^2) \tag{A10}$$

$$b_{j,4}=R_jC_j(r_j+L_j)+L_j \tag{A11}$$

$$b_{j,5}=a_{j,4} \tag{A12}$$

where $Y_j(s)$ is the input admittance of PM$_j$; $G_{j,\mathrm{d}}(s)$ is the voltage controller; d is the duty cycle of pulse-width modulation; $k_{j,\mathrm{da}}$ is the equivalent gain of the converter; R_j is the equivalent output resistance; L_j, C_j, and r_j are the inductance, capacitance, and resistance of the filter circuit, respectively; and $I_{j,\mathrm{c}}$ is the current of the filter inductance.

$$G_{j,\mathrm{pd}}(s)=\frac{c_{j,3}s^3+c_{j,2}s^2+c_{j,1}s^1+c_{j,0}}{b_{j,5}s^5+b_{j,4}s^4+b_{j,3}s^3+b_{j,2}s^2+b_{j,1}s^1+b_{j,0}} \tag{A13}$$

$$c_{j,0}=G_{j,\mathrm{d}}(s)k_{j,\mathrm{da}}[1+I_{j,\mathrm{c}}(R_j+r_j)] \tag{A14}$$

$$c_{j,1}=G_{j,\mathrm{d}}(s)k_{j,\mathrm{da}}[d+I_{j,\mathrm{c}}(R_j+r_j+L_j+R_jC_jr_j)] \tag{A15}$$

$$c_{j,2}=G_{j,\mathrm{d}}(s)k_{j,\mathrm{da}}I_{j,\mathrm{c}}(R_jC_jL_j+L_j+R_jC_jr_j)+G_{j,\mathrm{d}}(s)k_{j,\mathrm{da}}R_jC_jd \tag{A16}$$

$$c_{j,3}=G_{j,\mathrm{d}}(s)k_{j,\mathrm{da}}R_jC_jL_jI_{j,\mathrm{c}} \tag{A17}$$

where $G_{j,\mathrm{pd}}(s)$ is the closed-loop transfer function from the reference value in PM$_j$ of the output variables.

The implementation of RT Box experimental platform used in this paper is shown in Fig. A1.

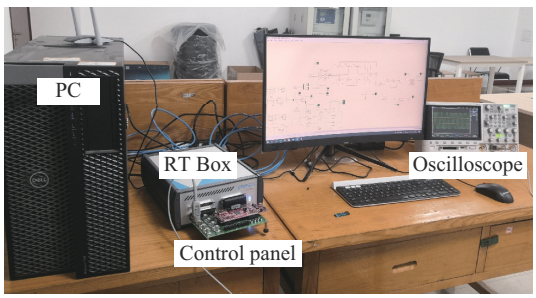

Fig. A1. Implementation of RT Box experimental platform.

REFERENCES

[1] C. Wang, W. Li, Y. Wang *et al*., "DC bus voltage fluctuation classification and restraint methods review for DC microgrid," *Proceedings of the CSEE*, vol. 37, no. 1, pp. 84-98, Jan. 2017.
[2] X. Yuan, S. Chen, and J. Hu, "Multi-scale voltage and power angle dynamic stability of power electronic power system," *Proceedings of the CSEE*, vol. 36, no. 19, pp. 5145-5154, Oct. 2016.
[3] K. Peng, J. Chen, B. Xu *et al*., "Key issues of stability and control in flexible DC distribution system," *Automation of Electric Power Systems*, vol. 43, no. 23, pp. 90-98, Dec. 2019.
[4] L. Guo, Y. Feng, X. Li *et al*., "Stability analysis and research of active damping method for DC microgrids," *Proceedings of the CSEE*, vol. 36, no. 4, pp. 927-936, Feb. 2016.
[5] L. Guo, P. Li, X. Li *et al*., "Reduced-order modeling and dynamic stability mechanism analysis of MTDC system in DC voltage control timescale," *CSEE Journal of Power and Energy Systems*, vol. 6, no. 3, pp. 591-600, Sept. 2020.
[6] G. Yao, K. Peng, H. Ling *et al*., "Reduced-order model and mechanism analysis of high-frequency oscillation in flexible DC distribution system," *Automation of Electric Power Systems*, vol. 44, no. 20, pp. 29-36, Oct. 2020.
[7] H. Li, K. Peng, Y. Chen *et al*., "Mechanism analysis of oscillation frequency of low frequency oscillation on DC voltage control time scale in DC distribution system," *High Voltage Engineering*, vol. 47, no. 6, pp. 2232-2242, Apr. 2021.
[8] H. Zhang, K. Peng, Y. Liu *et al*., "Low-frequency oscillation mechanism analysis of flexible DC distribution system based on MMC," *Electric Power Automation Equipment*, vol. 41, no. 5, pp. 22-28, Mar. 2021.
[9] D. Liu, L. Liu, H. Cheng *et al*., "An extended DC power flow model considering voltage magnitude," *Journal of Modern Power Systems and Clean Energy*, vol. 9, no. 3, pp. 679-683, May 2021.
[10] J. Liu, X. Huang, and Z. Li, "Multi-time scale optimal power flow strategy for medium-voltage DC power grid considering different operation modes," *Journal of Modern Power Systems and Clean Energy*, vol. 8, no. 1, pp. 46-54, Jan. 2020.
[11] M. N. Hamidi, D. Ishak, M. Zainuri *et al*., "Asymmetrical multi-level dc-link inverter for PV energy system with perturb and observe based voltage regulator and capacitor compensator," *Journal of Modern Power Systems and Clean Energy*, vol. 9, no. 1, pp. 199-209, Jan. 2021.
[12] L. Qiao, X. Li, D. Huang *et al*., "Coordinated control for medium voltage DC distribution centers with flexibly interlinked multiple microgrids," *Journal of Modern Power Systems and Clean Energy*, vol. 7, no. 3, pp. 599-611, May 2019.
[13] L. Zhang, Y. Chen, C. Shen *et al*., "Coordinated voltage regulation of hybrid AC/DC medium voltage distribution networks," *Journal of Modern Power Systems and Clean Energy*, vol. 6, no. 3, pp. 463-472, May 2018.
[14] N. Tsolas and P. Varaiya, "A structure preserving energy function for power system transient stability analysis," *IEEE Transactions on Circuits and Systems*, vol. 32, no. 10, pp. 1041-1049, Oct. 1985.
[15] L. Chen, Y. Chen, and W. Hu, "Low frequency oscillation analysis and oscillation source location based on oscillation energy. Part one: mathematical foundation and energy flow computation," *Automation of Electric Power Systems*, vol. 36, no. 3, pp. 22-27, Feb. 2012.
[16] L. Chen, Y. Chen, and W. Hu, "Low frequency oscillation analysis and oscillation source location based on oscillation energy. Part two: method for oscillation source location and case studies," *Automation of Electric Power Systems*, vol. 36, no. 4, pp. 1-5, Feb. 2012.
[17] Y. Shu, X. Zhou, and W. Li, "Analysis of low frequency oscillation and source location in power systems," *CSEE Journal of Power and Energy Systems*, vol. 4, no. 1, pp. 58-66, Mar. 2018.
[18] S. Sarmadi and V. Venkatasubramanian, "Inter-area resonance in power systems from forced oscillations," *IEEE Transactions on Power Systems*, vol. 31, no. 1, pp. 378-386, Jan. 2016.
[19] H. Shanechi, N. Pariz, and E. Vaahedi, "General nonlinear modal representation of large scale power systems," in *Proceedings of IEEE PES General Meeting*, Denver, USA, Jun. 2004, p. 1475.
[20] M. Wang and H. Sun, "An analysis method for forced power oscillation source detection," *Proceedings of the CSEE*, vol. 34, no. 34, pp. 6209-6215, Dec. 2014.
[21] S. Maslennikov, B. Wang, Z. Qiang *et al*., "A test cases library for methods locating the sources of sustained oscillations," in *Proceedings of IEEE PES General Meeting*, Boston, USA, Jul. 2016, pp. 17-21.
[22] U. Agrawal, J. Follum, D. Duan *et al*., "Locating the source of forced oscillations using PMU measurements and system model information,"

in *Proceedings of IEEE PES General Meeting*, Chicago, USA, Jul. 2017, pp. 1-5.
[23] N. Zhou, M. Ghorbaniparvar, and S. Akhlaghi, "Locating sources of forced oscillations using transfer functions," in *Proceedings of 2017 IEEE Power and Energy Conference at Illinois (PECI)*, Champaign, USA, Feb. 2017, pp. 1-8.
[24] M. Luan, J. Wu, S. Li *et al*., "Location method for forced oscillation source in mechanical parts based on frequency-domain characteristics of transfer function matrix," *Automation of Electric Power Systems*, vol. 43, no. 17, pp. 84-91, Sept. 2019.
[25] Y. LI, Y. Huang, J. Liu *et al*., "Power system oscillation source location based on damping torque analysis," *Power System Protection and Control*, vol. 43, no. 14, pp. 84-91, Jul. 2015.
[26] T. Jing and B. Liu, "Forced oscillation location in power systems using multiple empirical mode decomposition," *Proceedings of the CSEE*, vol. 42, no. 22, pp. 8063-8075, Nov. 2022.
[27] C. Wang, Y. Li, and K. Peng. "Overview of typical control methods for grid-connected inverters," *Proceedings of the CSU-EPSA*, vol. 24, no. 2, pp. 12-20, Apr. 2012.
[28] Y. Wang, X. Wang, F. Blaabjerg *et al*., "Harmonic stability analysis of inverter-fed power systems using component connection method," in *Proceedings of 2016 IEEE 8th International Power Electronics and Motion Control Conference*, Hefei, China, May 2016, pp. 2667-2674.
[29] P. Hou, E. Ebrahimzadeh, X. Wang *et al*., "Harmonic stability analysis of offshore wind farm with component connection method," in *Proceedings of 43rd Annual Conference of the IEEE Industrial Electronics Society*, Beijing, China, Oct. 2017, pp. 4926-4932.
[30] Y. Wang, X. Wang, Z. Chen *et al*., "Small-signal stability analysis of inverter-fed power systems using component connection method," *IEEE Transactions on Smart Grid*, vol. 9, no. 5, pp. 5301-5310, Sept. 2018.

Zida Zhao received the B.S. degree from Shandong University of Technology, Zibo, China, in 2018. He is currently pursuing the Ph.D. degree in electrical engineering in Shandong University of Technology. His research interest includes stability analysis of DC distribution network.

Ke Peng received the B.S. degree from China University of Mining and Technology, Xuzhou, China, in 2006, and the Ph.D. degree in electrical engineering from Tianjin University, Tianjin, China, in 2012. He is an Associate Professor at Shandong University of Technology, Zibo, China. His research interests include distributed generation system simulation, and AC/DC smart distribution system.

Richang Xian received the B.S. degree in electrical engineering from Shandong Polytechnic University, Jinan, China, in 1987, and the M.S. degree in electrical engineering from Huazhong University of Science and Technology, Hsinchu, China, in 2003. He is a Full Professor at Shandong University of Technology, Zibo, China, currently. His research interests include power system overvoltage, electrical equipment on-line monitoring and fault diagnosis technology.

Xinhui Zhang is a Full Professor and Master's Advisor at Shandong University of Technology, Zibo, China. Her research interests include fault detection and automation technology for distribution network, and grid-connected technology for distributed generation.